THE JOURNAL OF PHYSICAL CHEMISTRY B

Article

pubs.acs.org/JPCB

Ewald Electrostatics for Mixtures of Point and Continuous Line Charges

Hanne S. Antila,[†] Paul R. Van Tassel,[‡] and Maria Sammalkorpi*[,†]

[†]Department of Chemistry, Aalto University, 00076 Aalto, Finland

[‡]Department of Chemical & Environmental Engineering, Yale University, New Haven, Connecticut 06520, United States

ABSTRACT: Many charged macro- or supramolecular systems, such as DNA, are approximately rod-shaped and, to the lowest order, may be treated as continuous line charges. However, the standard method used to calculate electrostatics in molecular simulation, the Ewald summation, is designed to treat systems of point charges. We extend the Ewald concept to a hybrid system containing both point charges and continuous line charges. We find the calculated force between a point charge and (i) a continuous line charge and (ii) a discrete line charge consisting of uniformly spaced point charges to be numerically equivalent when the separation greatly exceeds the discretization length. At shorter separations, discretization induces deviations in the force and energy, and point charge−point charge correlation effects. Because significant computational savings are also possible, the continuous line charge Ewald method presented here offers the possibility of accurate and efficient electrostatic calculations.

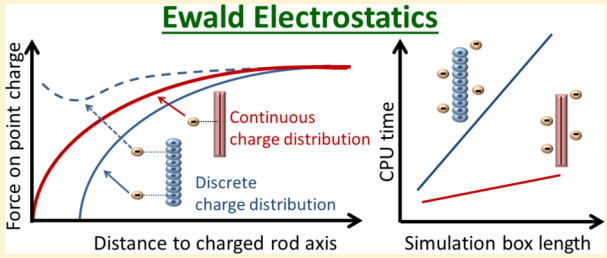

1. INTRODUCTION

Many important natural and synthetic macromolecular systems are charged and approximately one-dimensional (e.g., DNA, rigid polyelectrolytes, and charged nanotubes or nanorods). To a first approximation, the distribution of charge in these systems may be modeled as a continuous line charge. The behavior of one or more such line charges, together with neutralizing counterions and added electrolyte, may be predicted through various theoretical approaches, e.g., counterion condensation,[1,2] Poisson−Boltzmann,[3−6] density functional,[7] integral equation,[8,9] and strongly coupled Coulomb[4,10−13] theories. Of particular note are strongly coupled Coulomb predictions of overcharging and like-charge attraction,[10,12,14] features observed experimentally under strong coupling conditions (high charge or ion-valence)[15,16] yet in qualitative disagreement with many mean-field (e.g., Poisson−Boltzmann) approaches.

Molecular computer simulation can provide exact (within statistical uncertainty) results to which approximate theories, such as those referenced above, may be compared, and is thus an invaluable tool for testing and validating theoretical approaches. Simulation methods, such as molecular dynamics and Monte Carlo, require the calculation of intermolecular forces or energies, and in systems containing charged species, special care must be taken to accurately account for the long-range Coulomb interactions. The Ewald summation is currently the most widely used method for calculating electrostatic energies and forces within molecular systems containing point charges. Originally introduced in the context of crystalline structures,[17] the Ewald method works by adding and subtracting a Gaussian charge distribution around each point charge, resulting in two summations: one rapidly convergent in real space and the other in Fourier space. Many variants of the basic algorithm exist, both to optimize computational performance[18−20] and to account for different geometries.[21−25] In particular, Ewald-based methods have been derived for systems that are finite in some directions and periodic in others.[26,27] Despite impressive efforts to improve efficiency, calculating electrostatic interactions remains computationally expensive and is, appropriately, a topic of significant current interest.[28−31]

We present here an extension of the Ewald concept toward systems containing both line and point charges. Previous simulation studies of such systems have tended to employ cutoff schemes that essentially ignored the long-range nature of electrostatic forces,[8,32] or cylindrical cell models, where the infinite extent of a single line charge in the axial direction may be treated via a self-consistent mean-field scheme.[8,32−34] A variant of the MMM algorithm[35] has also been used to model a continuous line charge.[36] The Ewald-based method presented here applies to systems containing an arbitrary number of continuous line charges. Its most straightforward representation involves parallel line charges of infinite length within a periodic simulation cell, but a generalization for finite line charges of arbitrary length and even curvature is possible, although the results then become exact only in the (singular) limit of small Gaussian width.

The key motivation for developing this formalism is to enable the simulation of important idealized model systems (i.e., those containing continuous line charges) treated by many theories.

Received: August 6, 2015
Revised: September 7, 2015
Published: September 9, 2015

DOI: 10.1021/acs.jpcb.5b07637
J. Phys. Chem. B 2015, 119, 13218−13226

Previous comparisons to theories have involved simulations of discretely charged lines, where charge-discretization-based correlations may occur.[12,14,36,37] In particular, the surface charge distribution (i.e., the density, size, and location of discretized charge sites) has been observed to strongly influence the distribution of ions near a charged, planar surface[38] and spherical colloids.[39] In addition to polyelectrolyte (e.g., DNA) systems,[14,36] the proposed method could be used for coarse-grained representations of other rodlike biomolecules,[40−42] viruses,[43] coated and functionalized nanotubes,[44,45] liquid crystals,[46,47] and hydrogels.[48,49] Representing line charges within the Ewald framework potentially enables implementation as a simple extension to existing simulation packages.

Below, we derive Ewald-type expressions for the energy of a hybrid system consisting of discrete point and continuous line charges. We compare the results of continuous versus discretized Ewald summation in terms of the force exerted on a single point ion by a charged rod, the distribution of charged hard spheres around a charged rod, and the overall computational performance. We find the method to be accurate and computationally efficient compared to existing discrete Ewald-based methods.

2. THEORY

2.1. Electrostatic Basics. Consider a rectangular box of lengths L_x, L_y, and L_z and volume V containing a charge distribution $e\rho(\boldsymbol{r})$, with e being the elementary charge, such that $\int_V \rho(\boldsymbol{r})\mathrm{d}\boldsymbol{r} = 0$. Let the box be the central cell within a large number of identical boxes stacked in a space-filling arrangement and V' be the total volume of this collection of periodic boxes. A system formed in this way is periodic, so $\rho(\boldsymbol{r} + \boldsymbol{n}\cdot\mathbf{L}) = \rho(\boldsymbol{r})$, with $\boldsymbol{n} = n_x\hat{x} + n_y\hat{y} + n_z\hat{z}$ and the tensor $\mathbf{L} = L_x\hat{x}\hat{x} + L_y\hat{y}\hat{y} + L_z\hat{z}\hat{z}$. The mutually orthogonal unit vectors are denoted as $\hat{x}$, $\hat{y}$, and $\hat{z}$.

With the help of the Coulomb potential $\beta v(r) = e^2/(4\pi\epsilon k_\mathrm{b}Tr) = l_\mathrm{b}/r$, the electrostatic energy, U, due to interactions between charges in the central cell (of volume V) with charges in the extended collection of cells (of total volume V' and, hence, including the ions in the central cell), is obtained by integrating over the product of the charge distribution and the potential field $\phi(\boldsymbol{r})$ created by the charge distribution

$$\beta\phi(\boldsymbol{r}) = \int_{V'} \rho(\boldsymbol{r}')\beta v(|\boldsymbol{r} - \boldsymbol{r}'|)\,\mathrm{d}\boldsymbol{r}' \tag{1}$$

$$\begin{aligned}\beta U &= \frac{1}{2}\int_V \rho(\boldsymbol{r})\beta\phi(\boldsymbol{r})\,\mathrm{d}\boldsymbol{r}\\ &= \frac{1}{2}\int_V\int_{V'} \rho(\boldsymbol{r})\rho(\boldsymbol{r}')\beta v(|\boldsymbol{r} - \boldsymbol{r}'|)\,\mathrm{d}\boldsymbol{r}'\,\mathrm{d}\boldsymbol{r}\\ &= \frac{1}{2}\langle\rho|\beta v|\rho\rangle\end{aligned} \tag{2}$$

where $\beta = 1/k_\mathrm{b}T$, k_b is the Boltzmann constant, T is the temperature, and l_b is the Bjerrum length. The dielectric constant, ϵ, is assumed uniform. Note that integration over $\boldsymbol{r}$ and $\boldsymbol{r}'$extend over central cell (V) and collection of cells (V'), respectively. Any self energy is included in eq 2; we address this issue below for the specific cases of interest here. We introduce here a bracket notation $\langle\rho|\beta v|\rho\rangle$ as a convenient expression for the double integral.

By utilizing the Fourier transform of the Coulomb potential, $\beta\tilde{v}(k) = \frac{4\pi l_\mathrm{b}}{k^2}$, one can conveniently express the energy of eq 2 as a summation in reciprocal space:

$$\begin{aligned}\beta U &= \frac{1}{2V}\sum_{\boldsymbol{k}} \tilde{\rho}(-\boldsymbol{k})\beta\tilde{\phi}(\boldsymbol{k})\\ &= \frac{1}{2V}\sum_{\boldsymbol{k}} \tilde{\rho}(-\boldsymbol{k})\tilde{\rho}(\boldsymbol{k})\beta\tilde{v}(\boldsymbol{k})\\ &= \frac{2\pi l_\mathrm{b}}{V}\sum_{\boldsymbol{k}} \frac{1}{k^2}\tilde{\rho}(-\boldsymbol{k})\tilde{\rho}(\boldsymbol{k})\end{aligned} \tag{3}$$

where $\boldsymbol{k} = 2\pi\left[\frac{n'_x\hat{x}}{L_x} + \frac{n'_y\hat{y}}{L_y} + \frac{n'_z\hat{z}}{L_z}\right]$, with n'_x, n'_y, and n'_z being a set of integers, and the Fourier transform of periodic function $f(\boldsymbol{r})$ over volume V is defined as

$$\tilde{f}(\boldsymbol{k}) = \int_V f(\boldsymbol{r})\mathrm{e}^{-\mathrm{i}\boldsymbol{k}\cdot\boldsymbol{r}}\,\mathrm{d}\boldsymbol{r} \tag{4}$$

2.2. Ewald Summation of Point Charges. We first consider the case where the charge distribution consist of N_p point charges, each with position $\boldsymbol{r}_i$ and charge q_ie. The charge distribution ρ_p can be presented as

$$\rho_\mathrm{p} = \sum_{i=1}^{N_\mathrm{p}} q_i\delta(\boldsymbol{r} - \boldsymbol{r}_i) - \frac{1}{V}\sum_{i=1}^{N_\mathrm{p}} q_i \tag{5}$$

where $\delta(r)$ is the Dirac delta function, and an uniform background charge is subtracted to ensure electroneutrality. Direct calculation of the energy of a system corresponding to this charge distribution, by either eq 2 or eq 3, is impractical, owing to the $1/r$ form of the potential. The standard means of calculating energy is the Ewald summation[17] method, which involves dividing the charge distribution into two components, $\rho_\mathrm{p} = \rho_{\mathrm{p}1}+\rho_{\mathrm{p}2}$:

$$\rho_{\mathrm{p}1} = \frac{\alpha^3}{\pi^{3/2}}\sum_{i=1}^{N_\mathrm{p}} q_i\mathrm{e}^{-\alpha^2|\boldsymbol{r}-\boldsymbol{r}_i|^2} - \frac{1}{V}\sum_{i=1}^{N_\mathrm{p}} q_i \tag{6}$$

$$\rho_{\mathrm{p}2} = \sum_{i=1}^{N_\mathrm{p}} q_i\left[\delta(\boldsymbol{r} - \boldsymbol{r}_i) - \frac{\alpha^3}{\pi^{3/2}}\mathrm{e}^{-\alpha^2|\boldsymbol{r}-\boldsymbol{r}_i|^2}\right] \tag{7}$$

Note that Gaussian charge distributions are both added and subtracted from the charge distribution of eq 5 to yield eqs 6 and 7. The Gaussian contributions are essential for the efficient calculation of the electrostatics. These diffuse charge clouds, with width controlled by parameter α, screen the point charges such that the potential of $\rho_{\mathrm{p}2}$ rapidly decays and so may be evaluated as a sum in real space. Furthermore, the Fourier transforms of the compensating Gaussians, embedded in $\rho_{\mathrm{p}1}$, also decay quickly and yield a rapidly converging series in the Fourier space, thus facilitating the convergence of the total electrostatic energy $\beta U_{\mathrm{p}-\mathrm{p}} = \frac{1}{2}\langle\rho_\mathrm{p}|\beta v|\rho_{\mathrm{p}1}\rangle + \frac{1}{2}\langle\rho_\mathrm{p}|\beta v|\rho_{\mathrm{p}2}\rangle$.

The Fourier space (also referred as "reciprocal" or "k") contribution to the total energy reads

DOI: 10.1021/acs.jpcb.5b07637
J. Phys. Chem. B 2015, 119, 13218−13226

$$\beta U_{k,\mathrm{p-p}} = \frac{1}{2}\left\langle \rho_{\mathrm{p}} | \beta v | \rho_{\mathrm{p1}} \right\rangle = \frac{2\pi l_{\mathrm{b}}}{V} \sum_{\boldsymbol{k}\neq\boldsymbol{0}} \frac{\mathrm{e}^{-k^2/4\alpha^2}}{k^2} \sum_{i=1}^{N_{\mathrm{p}}} \sum_{j=1}^{N_{\mathrm{p}}} q_i q_j \mathrm{e}^{\mathrm{i}\boldsymbol{k}\cdot(\boldsymbol{r}_i - \boldsymbol{r}_j)} - \beta U_{\mathrm{self}} = \frac{2\pi l_{\mathrm{b}}}{V} \sum_{\boldsymbol{k}\neq\boldsymbol{0}} \frac{\mathrm{e}^{-k^2/4\alpha^2}}{k^2} \left[\left(\sum_{i=0}^{N_{\mathrm{p}}} q_i \cos(\boldsymbol{k}\cdot\boldsymbol{r}_i) \right)^2 + \left(\sum_{i=0}^{N_{\mathrm{p}}} q_i \sin(\boldsymbol{k}\cdot\boldsymbol{r}_i) \right)^2 \right] - \beta U_{\mathrm{self}} \tag{8}$$

The summation above includes the terms $i = j$ in the central cell of $\beta U_{k,\mathrm{p-p}}$. Therefore, the self-energy $\beta U_{\mathrm{self}} = \frac{\alpha l_{\mathrm{b}}}{\sqrt{\pi}} \sum_{i=1}^{N_{\mathrm{p}}} q_i^2$, due to the interaction between a Gaussian charge cloud and the point charge located in the center of that Gaussian, must be subtracted. βU_{self} is derived in section 2.4.

The remaining energetic terms can be determined via summations in real space:

$$\beta U_{r,\mathrm{p-p}} = \frac{1}{2}\left\langle \rho_{\mathrm{p}} | \beta v | \rho_{\mathrm{p2}} \right\rangle = \frac{1}{2} \sum_{\boldsymbol{n}} \sum_{i=1}^{N_{\mathrm{p}}} \sum_{j=1}^{N_{\mathrm{p}}}{}' q_i q_j \beta\phi_{\mathrm{p2}}(|\boldsymbol{r}_i - \boldsymbol{r}_j - \boldsymbol{n}\cdot\mathbf{L}|) + \frac{1}{2}\beta U_{\mathrm{p-p,bg}} \tag{9}$$

where the prime indicates the exclusion of the $i = j$ term when $\boldsymbol{n} = \boldsymbol{0}$. $\beta U_{\mathrm{p-p,bg}} = -\frac{\pi l_{\mathrm{b}}}{\alpha^2 V}\left[\sum_{i=1}^{N_{\mathrm{p}}} q_i\right]^2$ accounts for the interaction with the uniform, neutralizing background charge (see eq 6). The potential $\beta\phi_{\mathrm{p2}}(r)$ due to charge distribution $\rho_{\mathrm{p2}}(r)$ reads

$$\beta\phi_{\mathrm{p2}}(r) = \frac{l_{\mathrm{b}}}{r}\,\mathrm{erfc}(\alpha r) \tag{10}$$

The derivation of $\beta U_{\mathrm{p-p,bg}}$ and $\beta\phi_{\mathrm{p2}}(r)$ are presented in section 2.4. The total electrostatic energy of the system consisting of N_{p} point charges is given by

$$\beta U_{\mathrm{p-p}} = \beta U_{k,\mathrm{p-p}} + \beta U_{r,\mathrm{p-p}} \tag{11}$$

The point charge presentation discussed above is the standard way of formulating the Ewald sum. Similar derivations of the Ewald method applied to point charges can be found in standard texts.[50,51] Throughout this work, we employ the so-called "tinfoil" boundary conditions and assume that the collection of cubic cells is embedded in a perfect conductor.[50,52,53] This is the standard practice in most implementations of Ewald summation for molecular simulations[30] because nonconducting boundaries will create discontinuities in the energy when charges cross cell boundaries in 3D periodic systems (see ref 54 for recent discussion on the treatment of boundary conditions in Ewald summation).

2.3. Ewald Summation of Continuous Line Charges. Here, we modify this formulation to be applicable to a system consisting of N_{c} continuous line charges and N_{p} point charges. The total charge density of the system is now $\rho = \rho_{\mathrm{p}} + \rho_{\mathrm{c}}$, where ρ_{p} is given by eq 5 and

$$\rho_{\mathrm{c}}(\boldsymbol{r}) = \sum_{j=1}^{N_{\mathrm{c}}} \tau_j \left[\int_0^{L_j} \delta(\boldsymbol{r} - \boldsymbol{s}_j(s))\,\mathrm{d}s - \frac{L_j}{V} \right] \tag{12}$$

The trajectories of the line charges are here described as $\boldsymbol{s}_j(s) = x_j(s)\hat{x} + y_j(s)\hat{y} + z_j(s)\hat{z}$ where $x_j(s)$, $y_j(s)$, and $z_j(s)$ are in the most general case nonlinear functions of arc length s, such that $0 \le s \le L_j$, with L_j being the total arc length of line charge j and $1 \le j \le N_{\mathrm{c}}$. The charge per length of line charge j is denoted as τ_j.

As in the case of point charges in section 2.2, the charge density ρ_{c} can be divided into two contributions, $\rho_{\mathrm{c}} = \rho_{\mathrm{c1}} + \rho_{\mathrm{c2}}$, by adding and subtracting a Gaussian charge distribution

$$\rho_{\mathrm{c1}}(\boldsymbol{r}) = \sum_{j=1}^{N_{\mathrm{c}}} \tau_j \left[\frac{\alpha^3}{\pi^{3/2}} \int_0^{L_j} \mathrm{e}^{-\alpha^2|\boldsymbol{r}-\boldsymbol{s}_j(s)|^2}\,\mathrm{d}s - \frac{L_j}{V} \right] \tag{13}$$

$$\rho_{\mathrm{c2}}(\boldsymbol{r}) = \sum_{j=1}^{N_{\mathrm{c}}} \tau_j \int_0^{L_j} \left(\delta(\boldsymbol{r} - \boldsymbol{s}_j(s)) - \frac{\alpha^3 \mathrm{e}^{-\alpha^2|\boldsymbol{r}-\boldsymbol{s}_j(s)|^2}}{\pi^{3/2}} \right) \mathrm{d}s \tag{14}$$

The Fourier transform of eq 13 reads

$$\tilde{\rho}_{\mathrm{c1}}(\boldsymbol{k}) = 0 \qquad \boldsymbol{k} = \boldsymbol{0}$$
$$\tilde{\rho}_{\mathrm{c1}}(\boldsymbol{k}) = \mathrm{e}^{-k^2/4\alpha^2} \sum_{j=1}^{N_{\mathrm{c}}} \tau_j \int_0^{L_j} \mathrm{e}^{-\mathrm{i}\boldsymbol{k}\cdot\boldsymbol{s}_j}\,\mathrm{d}s \qquad \boldsymbol{k} \neq \boldsymbol{0} \tag{15}$$

The total energy of a system consisting of both line and point charges may be then expressed as

$$\beta U = \frac{1}{2}\left\langle \rho_{\mathrm{p}} + \rho_{\mathrm{c}} | \beta v | \rho_{\mathrm{p}} + \rho_{\mathrm{c}} \right\rangle = \frac{1}{2}\left\langle \rho_{\mathrm{p}} | \beta v | \rho_{\mathrm{p}} \right\rangle + \frac{1}{2}\left\langle \rho_{\mathrm{p}} | \beta v | \rho_{\mathrm{c}} \right\rangle + \frac{1}{2}\left\langle \rho_{\mathrm{c}} | \beta v | \rho_{\mathrm{p}} \right\rangle + \frac{1}{2}\left\langle \rho_{\mathrm{c}} | \beta v | \rho_{\mathrm{c}} \right\rangle \tag{16}$$

The contributions to the point charge−line charge energy due to the Gaussian charge distributions given by eqs 6 and 13 may be calculated via a summation in Fourier space

$$\beta U_{\mathrm{k,p-c}} = \frac{1}{2}\left\langle \rho_{\mathrm{p}} | \beta v | \rho_{\mathrm{c1}} \right\rangle + \frac{1}{2}\left\langle \rho_{\mathrm{c}} | \beta v | \rho_{\mathrm{p1}} \right\rangle = \frac{2\pi l_{\mathrm{b}}}{V} \sum_{\boldsymbol{k}\neq\boldsymbol{0}} \frac{\mathrm{e}^{-k^2/4\alpha^2}}{k^2} \sum_{i=1}^{N_{\mathrm{p}}} \sum_{j=1}^{N_{\mathrm{c}}} q_i \tau_j \left[\mathrm{e}^{\mathrm{i}\boldsymbol{k}\cdot\boldsymbol{r}_i} \int_0^{L_j} \mathrm{e}^{-\mathrm{i}\boldsymbol{k}\cdot\boldsymbol{s}_j}\,\mathrm{d}s + \mathrm{e}^{-\mathrm{i}\boldsymbol{k}\cdot\boldsymbol{r}_i} \int_0^{L_j} \mathrm{e}^{\mathrm{i}\boldsymbol{k}\cdot\boldsymbol{s}_j}\,\mathrm{d}s \right]$$
$$= \frac{4\pi l_{\mathrm{b}}}{V} \sum_{\boldsymbol{k}\neq\boldsymbol{0}} \frac{\mathrm{e}^{-k^2/4\alpha^2}}{k^2} \left(\left[\sum_{i=1}^{N_{\mathrm{p}}} q_i \cos(\boldsymbol{k}\cdot\boldsymbol{r}_i) \right] \times \left[\sum_{j=1}^{N_{\mathrm{c}}} \tau_j \int_0^{L_j} \cos(\boldsymbol{k}\cdot\boldsymbol{s}_j)\,\mathrm{d}s \right] + \left[\sum_{i=1}^{N_{\mathrm{p}}} q_i \sin(\boldsymbol{k}\cdot\boldsymbol{r}_i) \right] \left[\sum_{j=1}^{N_{\mathrm{c}}} \tau_j \int_0^{L_j} \sin(\boldsymbol{k}\cdot\boldsymbol{s}_j)\,\mathrm{d}s \right] \right) \tag{17}$$

Similarly, the contribution to the line charge−line charge energy due to the Gaussian charge distribution in eq 13 can be

DOI: 10.1021/acs.jpcb.5b07637
J. Phys. Chem. B 2015, 119, 13218−13226

obtained by

$$\beta U_{k,c-c} = \frac{1}{2}\langle \rho_c|\beta v|\rho_{c1}\rangle = \frac{2\pi l_b}{V}\sum_{\boldsymbol{k}\neq\boldsymbol{0}}\frac{e^{-k^2/4\alpha^2}}{k^2}\sum_{i=1}^{N_c}\sum_{j=1}^{N_c}\tau_i\tau_j \times \int_0^{L_i}\int_0^{L_j} e^{i\boldsymbol{k}\cdot(\boldsymbol{s}_i(s)-\boldsymbol{s}_j(s'))}\,ds'\,ds = \frac{2\pi l_b}{V}\sum_{\boldsymbol{k}\neq\boldsymbol{0}}\frac{e^{-k^2/4\alpha^2}}{k^2}\left(\left[\sum_{i=1}^{N_c}\tau_i\int_0^{L_i}\cos(\boldsymbol{k}\cdot\boldsymbol{s}_i)\,ds\right]^2 + \left[\sum_{i=1}^{N_c}\tau_i\int_0^{L_i}\sin(\boldsymbol{k}\cdot\boldsymbol{s}_i)\,ds\right]^2\right) \tag{18}$$

In the following, we assume the line charges to be parallel to the z direction and to span the central box (and thus to be infinite in the periodic system). The line charge trajectory is then written $\boldsymbol{s}_j(s) = x_j\hat{x} + y_j\hat{y} + s\hat{z}$, with x_j and y_j being constant. Taking into account the periodicity, $k_z = 2\pi/L_z$, the integral of eq 15 simplifies to

$$\int_0^{L_z} e^{-i\boldsymbol{k}\cdot\boldsymbol{s}_j}\,ds = e^{-i[k_x x_j + k_y y_j]}\int_0^{L_z} e^{-ik_z s}ds = \begin{cases} L_z e^{-i\boldsymbol{k}\cdot\boldsymbol{s}_j} & k_z = 0 \\ 0 & k_z \neq 0 \end{cases} \tag{19}$$

Consequently, the reciprocal space contributions to the energy, eqs 17 and 18, take the form

$$\beta U_{k,p-c} = \frac{4\pi l_b L_z}{V}\sum_{k_z=0,\boldsymbol{k}\neq\boldsymbol{0}}\frac{e^{-k^2/4\alpha^2}}{k^2}\sum_{i=1}^{N_p}\sum_{j=1}^{N_c} q_i\tau_j \times \cos(\boldsymbol{k}\cdot(\boldsymbol{r}_i - \boldsymbol{s}_j)) \tag{20}$$

$$\beta U_{k,c-c} = \frac{2\pi l_b L_z^2}{V}\sum_{k_z=0,\boldsymbol{k}\neq\boldsymbol{0}}\frac{e^{-k^2/4\alpha^2}}{k^2} \times \left[\left(\sum_{j=1}^{N_c}\tau_j\cos(\boldsymbol{k}\cdot\boldsymbol{s}_j)\right)^2 + \left(\sum_{j=1}^{N_c}\tau_j\sin(\boldsymbol{k}\cdot\boldsymbol{s}_j)\right)^2\right] \tag{21}$$

The remaining energy terms are calculated in real space

$$\beta U_{r,p-c} = \frac{1}{2}\left\langle \rho_p|\beta v|\rho_{c2}\right\rangle + \frac{1}{2}\left\langle \rho_c|\beta v|\rho_{p2}\right\rangle = l_b\sum_{\boldsymbol{n}}\sum_{i=1}^{N_p}\sum_{j=1}^{N_c} q_i\tau_j E_1(\alpha^2|\boldsymbol{r}_i - \boldsymbol{s}_j - \boldsymbol{n}\cdot\mathbf{L}|^2) + \frac{1}{2}\beta U_{p-c,bg} \tag{22}$$

$$\beta U_{r,c-c} = \frac{1}{2}\left\langle \rho_c|\beta v|\rho_{c2}\right\rangle = \frac{L_z l_b}{2}\sum_{\boldsymbol{n}}{\sum_{i=1}^{N_c}}'\sum_{j=1}^{N_c}\tau_i\tau_j E_1(\alpha^2|\boldsymbol{s}_i - \boldsymbol{s}_j - \boldsymbol{n}\cdot\mathbf{L}|^2) + \frac{1}{2}\beta U_{c-c,bg} \tag{23}$$

where the prime indicates omission of the $i = j$ contribution in the summation of eq 23. The terms $\beta U_{p-c,bg} = -\frac{2\pi l_b L_z}{\alpha^2 V}[\sum_{i=1}^{N_p} q_i][\sum_{j=1}^{N_c}\tau_j]$ and $\beta U_{c-c,bg} = -\frac{\pi l_b L_z^2}{\alpha^2 V}[\sum_{j=1}^{N_c}\tau_j]^2$ originate from the interactions with the uniform background charge and are derived in Section 2.4. E_1 is the exponential integral

$$E_1(x) = \int_x^\infty \frac{e^{-w}}{w}\,dw \tag{24}$$

The total electrostatic energy of the system now reads

$$\beta U = \beta U_{k,p-p} + \beta U_{r,p-p} + \beta U_{k,p-c} + \beta U_{r,p-c} + \beta U_{k,c-c} + \beta U_{r,c-c} \tag{25}$$

where the energy terms are given by eqs 8, 9, 20, 21, 22, and 23. Note that in the case of charge neutral systems, the net charge corrections embedded in eq 25 cancel.

2.4. Electrostatic Potentials. To derive the potential of eq 10, we first obtain the electric potential around a (3D) spherically symmetric Gaussian charge distribution by utilizing the Poisson equation

$$\frac{1}{r}\frac{d^2}{dr^2}(r\beta\phi_{G_{3D}}(r)) = -4\pi l_b\rho_{G_{3D}} = -\frac{4\alpha^2 l_b}{\sqrt{\pi}}e^{-\alpha^2 r^2} \tag{26}$$

$$\Rightarrow \beta\phi_{G_{3D}}(r) = \frac{l_b}{r}\,\mathrm{erf}(\alpha r) \tag{27}$$

where the erf(x) is the error function. The potential of a single unit point charge is $\beta\phi_p(r) = l_b/r$, and the potential of charge distribution ρ_{p2} (see eq 7), where a point charge is embedded in a screening Gaussian distribution, is therefore

$$\beta\phi_{p2}(r) = \beta\phi_p(r) - \beta\phi_{G_{3D}}(r) = \frac{l_b}{r}\,\mathrm{erfc}(\alpha r) \tag{28}$$

where the complementary error function, erfc(x), is defined as

$$\mathrm{erfc}(x) = \frac{2}{\sqrt{\pi}}\int_x^\infty e^{-t^2}\,dt \tag{29}$$

The self-interaction correction term, depicting the interaction of the Gaussian charge distributions with the point charges at their centers, is given in terms of $\beta\phi_{p2}(r)$ at $r = 0$

$$\beta U_{self} = \frac{1}{2}\lim_{r\to 0}\sum_{i=1}^{N_p} q_i^2\phi_{G_{3D}}(r) = \frac{\alpha l_b}{\sqrt{\pi}}\sum_{i=1}^{N_p} q_i^2 \tag{30}$$

and interaction of the screened point charge with the uniform charge background, needed for eq 9, may then be calculated via

DOI: 10.1021/acs.jpcb.5b07637
J. Phys. Chem. B 2015, 119, 13218−13226

$$\beta U_{\mathrm{p-p,bg}} = -\frac{1}{V}\left[\sum_{i=1}^{N_\mathrm{p}} q_i\right]^2 \int_0^\infty \beta\phi_{\mathrm{p2}}(\boldsymbol{r})\,\mathrm{d}\boldsymbol{r} = -\frac{\pi l_\mathrm{b}}{\alpha^2 V}\left[\sum_{i=1}^{N_\mathrm{p}} q_i\right]^2 \tag{31}$$

The correction terms relating to the line charge are derived using the same strategy. To calculate the electric potential due to the charge distribution ρ_{c2} (eq 14), we first consider the electric potential around a (2D) cylindrically symmetric Gaussian charge distribution of unit charge density. The electric potential is determined by the Poisson equation

$$\frac{1}{r}\frac{\mathrm{d}}{\mathrm{d}r}\left(r\frac{\mathrm{d}\beta\phi_{\mathrm{G_{2D}}}}{\mathrm{d}r}\right) = -4\pi l_\mathrm{b}\rho_{\mathrm{G_{2D}}}(r) = -4\alpha^2 l_\mathrm{b} \mathrm{e}^{-\alpha^2 r^2} \tag{32}$$

where r is now the distance to the center of cylindrical distribution. Integration yields

$$r\frac{\mathrm{d}\beta\phi_{\mathrm{G_{2D}}}}{\mathrm{d}r} = -2l_\mathrm{b}(1 - \mathrm{e}^{-\alpha^2 r^2}) \tag{33}$$

Similarly, the result for a continuous line charge is

$$\frac{\mathrm{d}\beta\phi_\mathrm{c}}{\mathrm{d}r} = \frac{2l_\mathrm{b}}{r} \tag{34}$$

After these expressions are combined, the potential for a line charge within an oppositely charged 2D Gaussian (ρ_{c2}; see eq 14) is

$$\frac{\mathrm{d}\beta\phi_{\mathrm{c2}}}{\mathrm{d}r} = \frac{\mathrm{d}\beta\phi_\mathrm{c}}{\mathrm{d}r} - \frac{\mathrm{d}\beta\phi_{\mathrm{G_{2D}}}}{\mathrm{d}r} = -2l_\mathrm{b}\frac{\mathrm{e}^{-\alpha^2 r^2}}{r} \tag{35}$$

$$\beta\phi_{\mathrm{c2}}(r) = 2l_\mathrm{b}\int_r^\infty \frac{\mathrm{e}^{-\alpha^2 r^2}}{r}\,\mathrm{d}r = l_\mathrm{b}E_1(\alpha^2 r^2) \tag{36}$$

where E_1 is the exponential integral given in eq 24. For the line charge, the terms relating to the interaction with uniform background charge are then

$$\beta U_{\mathrm{p-c,bg}} = -\frac{L_z}{V}\left[\sum_{i=1}^{N_\mathrm{p}} q_i\right]\left[\sum_{j=1}^{N_\mathrm{c}} \tau_j\right]\left[4\pi\int_0^\infty \beta\phi_{\mathrm{p2}}(r) r^2\,\mathrm{d}r + 2\pi\int_0^\infty \beta\phi_{\mathrm{c2}}(r) r\,\mathrm{d}r\right] = -\frac{2\pi l_\mathrm{b} L_z}{\alpha^2 V}\left[\sum_{i=1}^{N_\mathrm{p}} q_i\right]\left[\sum_{j=1}^{N_\mathrm{c}} \tau_j\right] \tag{37}$$

$$\beta U_{\mathrm{c-c,bg}} = -\frac{2\pi L_z^2}{V}\left[\sum_{j=1}^{N_\mathrm{c}} \tau_j\right]^2 \int_0^\infty \beta\phi_{\mathrm{c2}}(r) r\,\mathrm{d}r = -\frac{\pi l_\mathrm{b} L_z^2}{\alpha^2 V}\left[\sum_{j=1}^{N_\mathrm{c}} \tau_j\right]^2 \tag{38}$$

3. SIMULATION

We conduct Monte Carlo (MC) simulations on systems containing both charged rods and charged spheres. Charged rods span the simulation cell in the z direction and consist of either (i) continuous line charges surrounded by a hard cylinder (CONT) or (ii) lines of equally spaced discrete point charges, each surrounded by a hard sphere (DISC). These systems are fully consistent with the usual implementation of Ewald methods, where the excluded volume around a point charge is a sphere. In the limit of infinite discretization, the excluded volume of the DISC rod approaches that of a cylinder. The counter charge of the rods is introduced into the system as point charges, surrounded by a hard-sphere excluded volume.

In our simulations, the charged rods remain fixed in space, whereas the charged spheres sample phase space at random according to the standard Metropolis Monte Carlo (MC) algorithm. The Ewald formulations described in section 2 provide the system energy. The charged spheres representing the counter charge are initially placed at random, overlap-excluded positions in the simulation cell and allowed to equilibrate for at least 10^5 Monte Carlo steps. Following the initial equilibration, up to 10^8 steps are sampled to calculate the reported quantities.

Our test system could represent, e.g., the interactions between rigid polyelectrolytes and their counterions, and in the following, we refer to the mobile, discrete charges as ions. Our simulation parameters are chosen to represent typical experimental situation: the line charge density of $\tau = -4/l_\mathrm{b}$ and rod radius of either 0.3 l_b or 1.1 l_b approximate (linear) polyethylenimine and double-stranded DNA, respectively. The counterion radius of 0.3 l_b approximates the hydration radius of a small (e.g., sodium) ion.

A total of two different discretization densities are considered for the discrete charged rod, corresponding to point charge spacing of 0.4 l_b ($\mathrm{DISC_{SPARSE}}$) or 0.125 l_b ($\mathrm{DISC_{DENSE}}$). The simulation box is cubic and has a volume of $20 \times 20 \times 20\ l_\mathrm{b}^3$, and the rod(s) span the box in the z direction. Real-space cutoff r_cut of $L/2$, reciprocal space cutoff k_cut of 9, and the screening parameter α of $3.7/r_\mathrm{cut}$ are used as Ewald summation parameters for both the continuous and discretized presentations.

The 3D radial distribution function $g(r)$ is used to measure correlations between the rod charge and the charged spheres. It captures both the radial ion distribution and the organization of ions along the length of the rod. For the discrete charged rods, $g(r)$ is calculated between the centers of (i) charged sites on the rod and (ii) mobile charged spheres (ions), with r denoting the distance between the two. For the continuous-charged-rods model, $g(r)$ is calculated between (i) 100 artificial sites along the continuous line charge and (ii) the centers of the mobile charged spheres (ions). Note that because the line charge is uniform, the outcome is insensitive to the positions of the artificial sites.

To compare the computational scaling of the methods, we utilize a test system of two oppositely charged parallel rods with rod−rod separation of 5 l_b and charge per length $\tau = \pm 4/l_\mathrm{b}$. The rods are placed in a simulation box of $L \times L \times L$, spanning the box in the z direction. For both rods, $|\tau|L$ monovalent counterions are added ($|\tau|L$ anions and $|\tau|L$ cations). $\mathrm{DISC_{DENSE}}$ is used as rod charge discretization because it gives comparable results in terms of the ion distribution for the monovalent ion systems as the continuous line charge formulation. The CPU time of a MC simulation run is monitored for increasing L, while $k_\mathrm{cut} = 9$ is kept constant, and $r_\mathrm{cut} = L/2$ and $\alpha = 3.7/r_\mathrm{cut}$ are scaled accordingly. All of the MC simulations done in this work are conducted with a simple, direct implementation of Ewald summation (no meshing[55] is utilized in the reciprocal space).

DOI: 10.1021/acs.jpcb.5b07637
J. Phys. Chem. B 2015, 119, 13218−13226

4. RESULTS AND DISCUSSION

4.1. Ion Force. We begin by calculating the force between a single (continuous or discrete) line charge and a single point ion as a function of radial distance between the rod and the ion. For the discrete line charge, trajectories approaching the rod at an axial location of discretized charge, or a position directly between two discrete charges on the rod, are considered. In Figure 1,

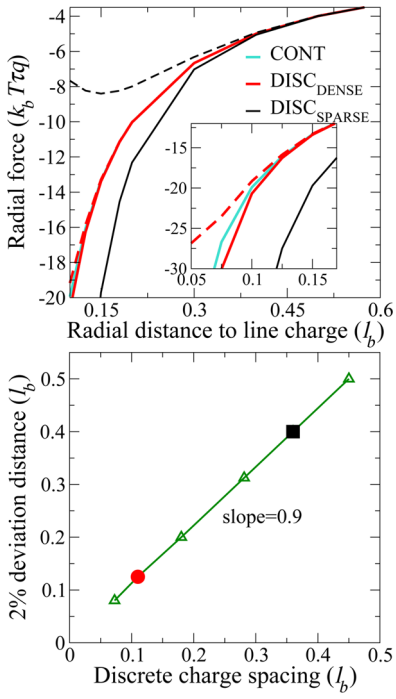

Figure 1. (Top) Scaled radial force between a point charge of valence q and a continuous (CONT), densely discrete (DISC$_{DENSE}$, charge separation of 0.125 l_b) or sparsely discrete (DISC$_{SPARSE}$, charge separation of 0.4 l_b) line charge of charge density τ. The point charge trajectory approaches either a discrete line charge (solid line) or a position between two discrete line charges (dashed line). Negative force indicates attraction. (Bottom) Distance at which the force deviates 2% from the CONT force, shown as a function of the discrete line charge spacing. DISC$_{SPARSE}$ is denoted with a filled square and DISC$_{DENSE}$ with a filled circle.

we show that discrete and continuous systems exhibit identical forces at a large separation within numerical accuracy. At shorter separations, some deviation is observed. The force produced by a sparsely discrete line charge (charge separation of 0.4 l_b) deviates significantly from one exerted by the continuous line charge at short separation, with the trajectory approaching a discretization site (a position between two sites) resulting in a much greater (lesser) magnitude of force. The densely discrete line charge (charge separation of 0.125 l_b) exhibits deviations from the continuous line charge only at very short separations. Figure 1 demonstrates that the point of deviation correlates with the discretization spacing: the separation where the discrete versus continuous force deviates by 2% is roughly equal to the spacing of the discretization sites along the rod. These results confirm the accuracy of the continuous line charge Ewald method and provide a clear indication of how line charge discretization affects the electrostatic forces.

4.2. Ion Distribution. To verify that the differences demonstrated in Figure 1 bear significance under realistic simulation conditions, we investigate the effect of the rod discretization on the counterion distributions around a single charged rod in a MC simulation.

In Figure 2, the radial distribution function between sites on the charged rod and either monovalent or trivalent counterions

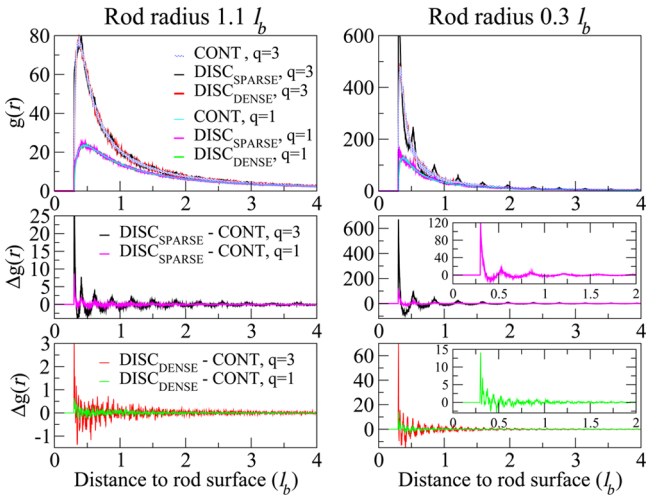

Figure 2. (Top) Radial distribution functions $g(r)$ between rod charges and counterions for continuously and discretely charged rods, as determined by Monte Carlo simulation. Rod charge density τ is $-4/l_b$, and ion radius is 0.3 l_b. The middle and bottom rows show differences in $g(r)$ between the continuously and discretely charged rods ($\Delta g(r)$).

are presented for different discretizations and rod radii. The data show that a dense enough rod charge discretization produces an ion distribution that is equivalent to that of a continuous line charge. This demonstrates that the two presented methods result in a numerically equivalent outcome if the line charge discretization is sufficiently dense.

In contrast, the DISC$_{SPARSE}$ system has clear differences from the DISC$_{DENSE}$ and CONT test systems. For $\tau = -4/l_b$, the radial distribution function of trivalent ions shows the emergence of a distinctive, long-ranged order between the discretized charge sites of the rod and the ions. The discretized representations also produce an ion distribution that is shifted slightly to a shorter distance compared to that of the CONT model. The ordering is diminished for monovalent counterions. Equivalently, no such ordering is detected when the coupling strength is decreased by changing the charge per length of the rod to $\tau = -1/l_b$ (data not shown). At a small rod radius, the correlations between the rod charge sites and the ions are considerably stronger, and as a result, the periodicity in the $g(r)$ is reliably detectable even for DISC$_{DENSE}$.

The spacing and locations of the $g(r)$ peaks reveal the long-range order in the radial distribution function to be due to counterions residing at axial locations between charged sites on the discretized rods. The ordering between the sites is caused by two mechanisms: (1) the energetic differences due to point charge−point charge correlations induced by the discretization of the rod charge (demonstrated in Figure 1) and (2) the difference in excluded volume between the models (cylinder versus overlapping spheres). For the rod with a radius of 1.1 l_b, the excluded volume effect is of order 0.01 k_bT, and the point charge correlations cause the long-range order. However, the organization of ions around the thinner rod is enhanced by both mechanisms.

We note that multivalent ions can form latticelike structures, driven by ion−ion electrostatic forces, even without a surface

DOI: 10.1021/acs.jpcb.5b07637
J. Phys. Chem. B 2015, 119, 13218−13226

charge discretization.[56−58] However, the distributions presented here specifically measure the rod−ion, not the ion−ion, structural correlations. Therefore, we have established above that rod charge discretization affects the ion placement near the charged rods. The effect is most pronounced for high line charge density, high ion valence, and small rod radius. Our results agree with prior findings of the effect of charge discretization on electric double layers near charged surfaces.[38] Furthermore, surface charge discretization has been shown to lead to a "pinned" structure, where counterions associate with surface charge sites[39] in a primitive model of spherical, charged colloids. Similar association is found here, although the ions preferentially reside between the discrete sites.

Charged cylinders, similar to the ones modeled here, have been widely used to study the counterintuitive DNA−DNA condensation (see, e.g., refs 36 and14). In these systems, the like-charge attraction involved with condensation has been suggested to be mediated by the latticelike organization of multivalent ions between the rods.[4,10,37] Our findings here demonstrate that discretization can have a notable effect on ion organization and, therefore, could influence the forces between two rods. To further investigate, we perform Monte Carlo simulations on a system of two like-charged rods, together with trivalent counterions, for both sparsely discretized and continuous rod charges and calculate the force between the rods as a function of rod separation (see Figure 3). The reported force includes both

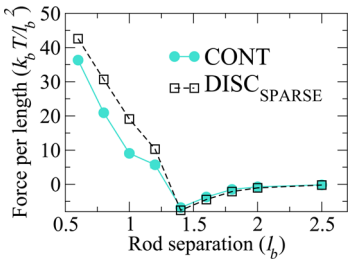

Figure 3. Force per length between two rods of radius 0.3 l_b and $\tau = -4/l_b$ charge per length in cases of continuous and discrete line charge. Rod charge is neutralized by trivalent counterions (radius 0.3 l_b). Positive force corresponds to repulsion between the rods, and the uncertainty in each data point is smaller than the symbol size. Rod separation is measured as the distance between the rod centers.

the electrostatic contribution from the Coulomb interactions (obtained by differentiating eq 25) and the kinetic contribution due to hard-core-repulsive interactions with counterions (calculated as in ref 14.). The force curves demonstrate that discretization and specific excluded volume can indeed affect not only the spatial distribution of the ions but also the resultant force between two charged rods. The difference in force is most pronounced at short rod separation. When the separation between the rod surfaces is smaller than the diameter of the ions, the forces can differ by several k_bT per unit length of the rod, thus significantly exceeding thermal energy.

4.3. Computational Load. Finally, we investigate the computational load of simulations employing continuous versus discrete line charge. We note that the computational benefit of a continuous presentation compared to a discrete one is highly dependent on the system studied, and therefore, the purpose of this section is to provide a rough order-of-magnitude estimate of the difference in scaling. We choose to investigate the computational cost of an MC simulation of two oppositely charged rods with $\tau = \pm 4/l_b$ and their $N_c = 2|\tau|L$ monovalent counterions. To obtain the data of Figure 4, we time the run of

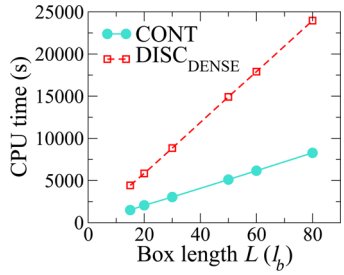

Figure 4. CPU time consumption of 30 000 Monte Carlo steps in a simulation of two oppositely charged rods with charge density $\tau = \pm 4/l_b$ and their monovalent counterions. Each data point is run as a single processor job.

the code from start to finish, and we note that several additional optimizations, which are not related to Ewald summation, are possible in the implementation of the code when switching from discretized to continuous line charge presentation, but the differences seen in Figure 4 predominantly originate from the Ewald part of the code, not from, e.g., input−output efficiency.

We observe an increase by a factor of 3 in computational efficiency with the continuous distribution due to the computational load of calculating additional pairwise interactions in the discrete system. As the number of such interactions increases with L, the (absolute) benefit in using the continuous line charge formulation in comparison to the discretized formulation is most pronounced for larger box lengths. Larger box sizes are often needed, e.g., when one wants to eliminate artifacts originating from box periodicity or finite size. An example is the ion condensation to polyelectrolytes in dilute solutions.[13]

The linear scaling of computational time versus box length L can be explained as follows. First, the energy of a particular Monte Carlo move is decomposable into a static and a locally changing part within the straightforward implementation of Ewald summation. Second, the value of α and r_{cut} are chosen to scale with box length and with such magnitude that the real space contributions can be calculated using the central cell only (minimum image convention). Therefore, calculating the energy difference during each Monte Carlo move requires time of order $N_p + N_c$. In our specific application of the system representing charged polymers and their counterions, this translates to linear scaling as a function of box length L.

As a consequence, the ratio of efficiency of the continuous and the discrete line charge presentation scales as $(N_p + N_cL/\Delta)/(N_p + N_c)$ or, assuming $N_p \gg N_c$, roughly as $1+N_cq/\tau\Delta$, where Δ is the discretization spacing. This relation predicts a factor of 3 difference in scaling in favor of the continuous model for the systems studied in Figure 4, which is perfectly in line with our results. For increasing number of point charges N_p (for example, a high concentration of added salt), both the discrete and the continuous Ewald summation become equally inefficient, as the point−point interactions dominate the CPU time consumption. Accordingly, for systems with a large number of point charges, utilizing a straightforward implementation of the Ewald summation (continuous or discretized) is not advisable. Instead, switching to techniques that employ meshing (see, e.g., ref 55) is highly recommended. Conversely, for an increase in the number of line charges in the system (e.g., increasing polyelectrolyte

DOI: 10.1021/acs.jpcb.5b07637
J. Phys. Chem. B 2015, 119, 13218−13226

concentration or DNA bundle size), the continuous line charge Ewald method would produce around an improvement in computational scaling of a factor of $1 + 1/\tau\Delta$.

5. CONCLUSIONS

We present here an Ewald-based formalism for electrostatic calculations within systems containing point charges and continuous line charges. Accuracy is established by comparing the forces on a point charge, exerted by (i) a continuous line charge using the method formulated here and (ii) a discrete line charge using the standard Ewald method. Simulations of hard-sphere counterions around continuous versus discrete line charges reveal significant differences (in both the counterion structure and the force between line charges) for cases of high line charge density, multivalent counterions, and sparse discretization. The continuous line charge Ewald-based method presented here offers the possibility of accurate and efficient electrostatic calculations, enabling the direct simulation of systems commonly treated theoretically, as well as the efficient simulation of a variety of coarse-grained macromolecular systems.

AUTHOR INFORMATION

Corresponding Author

*E-mail: maria.sammalkorpi@aalto.fi.

Notes

The authors declare no competing financial interest.

ACKNOWLEDGMENTS

This research was supported by Academy of Finland, American Chemical Society's Petroleum Research Fund grant no. 47776-AC5, Aalto University School of Chemical Technology Doctoral Programme, and a Marie Curie Career Integration Grant within the Seventh European Community Framework Programme under grant agreement 293861. This work also benefited from the computational facilities and staff at CSC IT Centre for Science, Finland, and at the Yale University Faculty of Arts and Sciences High Performance Computing Centre, USA. The authors thank Prof. Mikko Karttunen for providing the original discrete Ewald summation code and Dr. Matej Kanduč for useful discussions.

REFERENCES

(1) Manning, G. S. Limiting Laws and Counterion Condensation in Polyelectrolyte Solutions. I. Colligative Properties. *J. Chem. Phys.* **1969**, *51*, 924−933.

(2) Manning, G. S. The Critical Onset of Counterion Condensation: A Survey of Its Experimental and Theoretical Basis. *Ber. Bunsenges. Phys. Chem.* **1996**, *100*, 909−922.

(3) Bret, M. L.; Zimm, B. H. Distribution of Counterions Around a Cylindrical Polyelectrolyte and Manning's Condensation Theory. *Biopolymers* **1984**, *23*, 287−312.

(4) Rouzina, I.; Bloomfield, V. A. Macroion Attraction Due to Electrostatic Correlation between Screening Counterions. 1. Mobile Surface-Adsorbed Ions and Diffuse Ion Cloud. *J. Phys. Chem.* **1996**, *100*, 9977−9989.

(5) Harries, D. Solving the Poisson-Boltzmann Equation for Two Parallel Cylinders. *Langmuir* **1998**, *14*, 3149−3152.

(6) Deserno, M.; Holm, C.; May, S. Fraction of Condensed Counterions around a Charged Rod: Comparison of Poisson-Boltzmann Theory and Computer Simulations. *Macromolecules* **2000**, *33*, 199−206.

(7) Patra, C.; Bhuiyan, L. The Effect of Ionic Size on Polyion-Small Ion Distributions in a Cylindrical Double Layer. *Condens. Matter Phys.* **2005**, *8*, 425−446.

(8) Murthy, C. S.; Bacquet, R. J.; Rossky, P. J. Ionic Distributions near Polyelectrolytes. A Comparison of Theoretical Approaches. *J. Phys. Chem.* **1985**, *89*, 701−710.

(9) Shew, C.-Y.; Yethiraj, A. Computer Simulations and Integral Equation Theory for the Structure of Salt-free Rigid Rod Polyelectrolyte Solutions: Explicit Incorporation of Counterions. *J. Chem. Phys.* **1999**, *110*, 11599−11607.

(10) Shklovskii, B. Wigner Crystal Model of Counterion Induced Bundle Formation of Rodlike Polyelectrolytes. *Phys. Rev. Lett.* **1999**, *82*, 3268−3271.

(11) Shklovskii, B. I. Screening of a Macroion by Multivalent Ions: Correlation-induced Inversion of Charge. *Phys. Rev. E: Stat. Phys., Plasmas, Fluids, Relat. Interdiscip. Top.* **1999**, *60*, 5802−5811.

(12) Naji, A.; Arnold, A.; Holm, C.; Netz, R. R. Attraction and Unbinding of Like-Charged Rods. *Europhys. Lett.* **2004**, *67*, 130−136.

(13) Naji, A.; Netz, R. R. Counterions at Charged Cylinders: Criticality and Universality beyond Mean-Field Theory. *Phys. Rev. Lett.* **2005**, *95*, 185703.

(14) Kanduč, M.; Naji, A.; Podgornik, R. Counterion-mediated Weak and Strong Coupling Electrostatic Interaction Between Like-charged Cylindrical Dielectrics. *J. Chem. Phys.* **2010**, *132*, 224703.

(15) Bloomfield, V. A. DNA Condensation by Multivalent Cations. *Biopolymers* **1997**, *44*, 269−282.

(16) Butler, J. C.; Angelini, T.; Tang, J. X.; Wong, G. C. L. Ion Multivalence and Like-Charge Polyelectrolyte Attraction. *Phys. Rev. Lett.* **2003**, *91*, 028301.

(17) Ewald, P. P. Die Berechnung Optischer und Elektrostatischer Gitterpotentiale. *Ann. Phys.* **1921**, *369*, 253−287.

(18) Essmann, U.; Perera, L.; Berkowitz, M. L.; Darden, T.; Lee, H.; Pedersen, L. G. A Smooth Particle Mesh Ewald Method. *J. Chem. Phys.* **1995**, *103*, 8577−8593.

(19) Darden, T.; York, D.; Pedersen, L. Particle Mesh Ewald: An N*log(N) Method for Ewald Sums in Large Systems. *J. Chem. Phys.* **1993**, *98*, 10089−10092.

(20) Hockney, R. W.; Eastwood, J. W. *Computer Simulation Using Particles*; CRC Press: New York, 1988.

(21) Osychenko, O.; Astrakharchik, G.; Boronat, J. Ewald Method for Polytropic Potentials in Arbitrary Dimensionality. *Mol. Phys.* **2012**, *110*, 227−247.

(22) Yang, W.; Jin, X.; Liao, Q. Ewald Summation for Uniformly Charged Surface. *J. Chem. Theory Comput.* **2006**, *2*, 1618−1623.

(23) De Leeuw, S. W.; Perram, J. W. Electrostatic Lattice Sums for Semi-infinite Lattices. *Mol. Phys.* **1979**, *37*, 1313−1322.

(24) Lindbo, D.; Tornberg, A.-K. Fast and Spectrally Accurate Ewald Summation for 2-periodic Electrostatic Systems. *J. Chem. Phys.* **2012**, *136*, 164111.

(25) Pan, C.; Hu, Z. Rigorous Error Bounds for Ewald Summation of Electrostatics at Planar Interfaces. *J. Chem. Theory Comput.* **2014**, *10*, 534−542.

(26) Tuckerman, M.; Minary, P.; Pihakari, K.; Martyna, G. In *Computational Methods for Macromolecules: Challenges and Applications*; Schlick, T., Gan, H., Eds.; Lecture Notes in Computational Science and Engineering; Springer: Berlin Heidelberg, 2002; Vol. *24*; pp 381−410.

(27) Yeh, I.-C.; Berkowitz, M. L. Ewald Summation for Systems With Slab Geometry. *J. Chem. Phys.* **1999**, *111*, 3155−3162.

(28) Toukmaji, A.; Board, J. A., Jr. Ewald Summation Techniques in Perspective: a Survey. *Comput. Phys. Commun.* **1996**, *95*, 73−92.

(29) Sagui, C.; Darden, T. A. Molecular Dynamics Simulations of Biomolecules: Long-Range Electrostatic Effects. *Annu. Rev. Biophys. Biomol. Struct.* **1999**, *28*, 155−179.

(30) Karttunen, M.; Rottler, J.; Vattulainen, I.; Sagui, C. In *Computational Modeling of Membrane Bilayers*; Feller, S. E., Ed.; Current Topics in Membranes;, Academic Press: San Diego, California, 2008; Vol. *60*; pp 49−89.

DOI: 10.1021/acs.jpcb.5b07637
J. Phys. Chem. B 2015, 119, 13218−13226

(31) Cisneros, G. A.; Karttunen, M.; Ren, P.; Sagui, C. Classical Electrostatics for Biomolecular Simulations. *Chem. Rev.* **2014**, *114*, 779−814.
(32) Mills, P.; Anderson, C. F.; Record, M. T. Monte Carlo Studies of Counterion-DNA Interactions. Comparison of the Radial Distribution of Counterions with Predictions of Other Polyelectrolyte Theories. *J. Phys. Chem.* **1985**, *89*, 3984−3994.
(33) Das, T.; Bratko, D.; Bhuiyan, L. B.; Outhwaite, C. W. Modified Poisson-Boltzmann Theory Applied to Linear Polyelectrolyte Solutions. *J. Phys. Chem.* **1995**, *99*, 410−418.
(34) Goel, T.; Patra, C. N.; Ghosh, S. K.; Mukherjee, T. Structure of Cylindrical Electric Double Layers: A Systematic Study by Monte Carlo Simulations and Density Functional Theory. *J. Chem. Phys.* **2008**, *129*, 154906.
(35) Arnold, A.; Holm, C. MMM2D: A fast and Accurate Summation Method for Electrostatic Interactions in 2D Slab Geometries. *Comput. Phys. Commun.* **2002**, *148*, 327−348.
(36) Deserno, M.; Arnold, A.; Holm, C. Attraction and Ionic Correlations between Charged Stiff Polyelectrolytes. *Macromolecules* **2003**, *36*, 249−259.
(37) Grønbech-Jensen, N.; Mashl, R.; Bruinsma, R.; Gelbart, W. Counterion-Induced Attraction between Rigid Polyelectrolytes. *Phys. Rev. Lett.* **1997**, *78*, 2477−2480.
(38) Madurga, S.; Martín-Molina, A.; Vilaseca, E.; Mas, F.; Quesada-Pérez, M. Effect of the Surface Charge Discretization on Electric Double Layers: A Monte Carlo Simulation Study. *J. Chem. Phys.* **2007**, *126*, 234703.
(39) Messina, R.; Holm, C.; Kremer, K. Effect of Colloidal Charge Discretization in the Primitive Model. *Eur. Phys. J. E: Soft Matter Biol. Phys.* **2001**, *4*, 363−370.
(40) Sanders, L. K.; Xian, W.; Guáqueta, C.; Strohman, M. J.; Vrasich, C. R.; Luijten, E.; Wong, G. C. L. Control of Electrostatic Interactions Between F-actin and Genetically Modified Lysozyme in Aqueous Media. *Proc. Natl. Acad. Sci. U. S. A.* **2007**, *104*, 15994−15999.
(41) Rossi, L.; Sacanna, S.; Velikov, K. P. Cholesteric Colloidal Liquid Crystals from Phytosterol Rod-like Particles. *Soft Matter* **2011**, *7*, 64−67.
(42) Zambito, A. M.; Knipling, L.; Wolff, J. Charge Variants of Tubulin, Tubulin S, Membrane-bound and Palmitoylated Tubulin from Brain and Pheochromocytoma cells. *Biochim. Biophys. Acta, Proteins Proteomics* **2002**, *1601*, 200−207.
(43) Zhang, Z.; Grelet, E. Tuning Chirality in the Self-assembly of Rod-like Viruses by Chemical Surface Modifications. *Soft Matter* **2013**, *9*, 1015−1024.
(44) Hwang, J.-Y.; Eltohamy, M.; Kim, H.-W.; Shin, U. S. Self Assembly of Positively Charged Carbon Nanotubes with Oppositely Charged Metallic Surface. *Appl. Surf. Sci.* **2012**, *258*, 6455−6459.
(45) Ioniţă, M.; Prună, A. Polypyrrole/carbon Nanotube Composites: Molecular Modeling and Experimental Investigation as Anti-corrosive Coating. *Prog. Org. Coat.* **2011**, *72*, 647−652.
(46) Liu, B.; Besseling, T. H.; Hermes, M.; Demirors, A. F.; Imhof, A.; van Blaaderen, A. Switching Plastic Crystals of Colloidal Rods with Electric Fields. *Nat. Commun.* **2014**, *5*, 3092.
(47) Shimura, H.; Yoshio, M.; Hoshino, K.; Mukai, T.; Ohno, H.; Kato, T. Noncovalent Approach to One-Dimensional Ion Conductors: Enhancement of Ionic Conductivities in Nanostructured Columnar Liquid Crystals. *J. Am. Chem. Soc.* **2008**, *130*, 1759−1765.
(48) Ostroha, J.; Pong, M.; Lowman, A.; Dan, N. Controlling the Collapse/Swelling Transition in Charged Hydrogels. *Biomaterials* **2004**, *25*, 4345−4353.
(49) Liu, X.; Tong, Z.; Hu, O. Swelling Equilibria of Hydrogels with Sulfonate Groups in Water and in Aqueous Salt Solutions. *Macromolecules* **1995**, *28*, 3813−3817.
(50) Frenkel, D.; Smit, B. *Understanding Molecular Simulation: from Algorithms to Applications*; Academic Press: San Diego, California, 2001; Vol. *1*.
(51) Allen, M. P.; Tildesley, D. J. *Computer Simulation of Liquids*; Oxford Science Publications/Oxford University Press: New York, 1989.
(52) De Leeuw, S.; Perram, J. Computer Simulation of Ionic Systems. Influence of Boundary Conditions. *Phys. A* **1981**, *107*, 179−189.
(53) Giese, T. J.; Panteva, M. T.; Chen, H.; York, D. M. Multipolar Ewald Methods, 1: Theory, Accuracy, and Performance. *J. Chem. Theory Comput.* **2015**, *11*, 436−450.
(54) Hu, Z. Infinite Boundary Terms of Ewald Sums and Pairwise Interactions for Electrostatics in Bulk and at Interfaces. *J. Chem. Theory Comput.* **2014**, *10*, 5254−5264.
(55) Deserno, M.; Holm, C. How to Mesh up Ewald Sums. I. A Theoretical and Numerical Comparison of Various Particle Mesh Routines. *J. Chem. Phys.* **1998**, *109*, 7678−7693.
(56) Perel, V.; Shklovskii, B. Screening of a Macroion by Multivalent ions: a New Boundary Condition for the Poisson-Boltzmann Equation and Charge Inversion. *Phys. A* **1999**, *274*, 446−453.
(57) Grosberg, A.; Nguyen, T.; Shklovskii, B. Colloquium: The Physics of Charge Inversion in Chemical and Biological Systems. *Rev. Mod. Phys.* **2002**, *74*, 329−345.
(58) Quesada-Pérez, M.; González-Tovar, E.; Martín-Molina, A.; Lozada-Cassou, M.; Hidalgo-Álvarez, R. Overcharging in Colloids: Beyond the Poisson-Boltzmann Approach. *ChemPhysChem* **2003**, *4*, 234−248.

DOI: 10.1021/acs.jpcb.5b07637
J. Phys. Chem. B 2015, 119, 13218−13226